Experimental Evaluation of Deadbeat Running on the ATRIAS Biped

William C. Martin[1], Albert Wu[1], and Hartmut Geyer[1]

***Abstract*—Theoretical spring mass models with deadbeat foot placement policies reveal very robust running in the presence of large and frequent, unexpected gait disturbances. Although this performance goes beyond what has been demonstrated on running machines, a transfer of this theory has only been investigated for simplified monopod systems. Here we investigate how well the control strategies developed for the spring mass model transfer to more complex and human-like robots. We use a model-based control framework to implement the spring mass behavior on a bipedal robot of human scale and weight with articulated legs and an actively stabilized trunk. Evaluating the tracking performance in robot experiments on undisturbed and disturbed running, we find that our controller achieves tracking consistent with the underlying model for velocity changes of $\pm 0.2\,\mathrm{m}\cdot\mathrm{s}^{-1}$. For larger velocity changes and ground height disturbances up to $\pm 15\,\mathrm{cm}$, the controller performance degrades but the robot maintains running. Based on perturbed simulations of the simplified model, we conclude that the degradation is largely related to force disturbances not considered in the underlying spring mass control theory. The results highlight both limitations of the existing spring mass theory for control of more complex machines and an SMM-based control that generates robust and versatile behavior in running robots.**

***Index Terms*—Humanoid and Bipedal Locomotion, Humanoid Robots, Underactuated Robots**

I. INTRODUCTION

THE simple spring mass model (SMM) describes a point mass rebounding on massless spring legs. Research on this model has led to deadbeat foot placement strategies that produce highly robust SMM running in the presence of large and frequent, unexpected gait disturbances [1]–[4]. This theoretical performance goes far beyond what has been demonstrated in running robots [5]–[8]. However, these robots are clearly more complex systems than the conceptual SMM. They possess more degrees of freedom leading to additional dynamics, are limited by actuator saturation, and experience sensory noise that produces uncertainty about the actual state of the system. As a result, the utility of SMM theories for the control of complex running robots remains largely unclear.

Addressing this gap in understanding, several researchers have investigated the foot placement strategies of the SMM on more simplified hopping robots. For an early example, Zeglin [9] investigated state space planning algorithms based on the SMM for a bow-legged hopper with a compressible spring and passively stabilized trunk. More recently, Shemer and Degani [10] investigated deadbeat hopping policies for a similar monopod robot with a gyroscopically stabilized trunk in a low gravity environment. They used an analytical approximation of the SMM to compare the effect of constant deadbeat impact angles to swing leg retraction policies. Finally, Uyanık and colleagues [11] quantified the predictive performance of analytical approximations of the SMM in achieving deadbeat behavior using a monopedal spring leg with no attached trunk. All these studies have in common that they were performed with small and specialized one-legged platforms, characterized by prismatic legs, passively stabilized trunk motion in stance, and external sensor measurements. In contrast, we are interested in understanding if the SMM leg placement theories can be transferred to more humanoid robots and attempt the transfer on ATRIAS, a bipedal machine of human scale and weight with an actively controlled trunk and without external sensing (Fig. 1).

For the transfer, we focus on rendering the best possible behavior match between the SMM and ATRIAS. To achieve this goal, we use a model-based force control approach during the stance phase of running. Controllers of this type have been implemented successfully on legged robots for tracking desired forces during locomotion [12]–[14]. Combined with tracking the deadbeat foot placements of the SMM in flight, ATRIAS should match the behavior and robustness observed in the simplified model. However, we expect deviations from this ideal behavior due to the real world challenges faced by the machine. We perform planar running experiments to quantify these deviations, and thus, the utility of the SMM theories for more complex robots.

The remainder of this paper is organized in four parts. We first provide a general overview of our control approach in section II before detailing its implementation on ATRIAS in section III. We then present the results of the running experiments in section IV, which show that the resulting controller achieves velocity tracking that is consistent with deadbeat behavior of the underlying model for velocity changes of $\pm 0.2\,\mathrm{m}\cdot\mathrm{s}^{-1}$. For larger velocity changes and ground height disturbances up to $\pm 15\,\mathrm{cm}$, the controller performance degrades, although the robot maintains running. We discuss the reasons for this degradation and highlight in section V directions to improve on these initial results about SMM-based control for generating robust and versatile behavior in running robots.

Manuscript received: September, 10, 2016; Revised November, 28, 2016; Accepted January, 1, 2017.

This paper was recommended for publication by Editor N. Tsagarakis upon evaluation of the Associate Editor and Reviewers' comments. This work was supported in part by the US National Science Foundation (CPS-1239143 and IIS-1563807).

[1]All authors are with The Robotics Institute, Carnegie Mellon University, 5000 Forbes Avenue, Pittsburgh, PA 15213, USA. {wmartin,apwu,hgeyer}@cmu.edu

Digital Object Identifier (DOI): see top of this page.

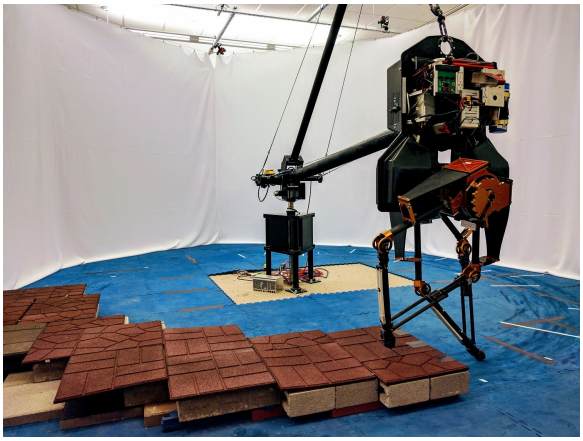

Fig. 1. CMU's ATRIAS biped shown in the boom testbed during the ground disturbance experiments with unexpected height changes of ±15 cm (discussed in section IV-C).

II. CONTROL APPROACH

The SMM consists of a point mass m rebounding on a massless spring leg of stiffness k and rest length l_0. This system behaves as a purely ballistic projectile during flight and as a spring-loaded inverted pendulum during stance with

$$\begin{aligned} m\ddot{x} &= k\left[l_0\,(x^2+z^2)^{-1/2}-1\right]x, \\ m\ddot{z} &= k\left[l_0\,(x^2+z^2)^{-1/2}-1\right]z - mg, \end{aligned} \tag{1}$$

where (x, z) are the coordinates of the point mass in the horizontal and vertical dimensions. The model does not consider sliding during stance. Stance occurs when the foot point strikes the ground and flight resumes once the leg length reaches l_0 during rebound. The model's trajectory in flight is fully determined by the horizontal speed $\dot{x}$ and the system energy E_s, which is a constant parameter of the model. Given the speed in one flight phase, the model behavior in the ensuing stance and flight phases is controlled by the leg angle α_{TD} at touchdown [2]. This influence of the landing angle on the model behavior can be captured with the apex return map, $\dot{x}_{i+1} = f(\dot{x}_i, \alpha_{\mathrm{TD},i})$, which relates the state of the model between the apexes of two subsequent flight phases (i and $i+1$). Inverting this function yields a deadbeat touchdown angle that takes the system from the current forward velocity $\dot{x}_i$ to a desired forward velocity $\dot{x}_{i+1} = \dot{x}_a^*$ in a single step,

$$\alpha^*_{\mathrm{TD},i} = f^{-1}(\dot{x}_i, \dot{x}^*_a). \tag{2}$$

Deadbeat controllers based on this theory have been identified that provide robustness to unobserved rough terrain for the SMM in simulation [2]–[4].

Our target platform for translating this theory is CMU's ATRIAS (Fig. 1), one of three identical copies of a human-sized bipedal robot developed by the Dynamic Robotics Laboratory at Oregon State University [15]. The centroidal dynamics of ATRIAS has inertial properties similar to that of human locomotion. The robot weighs about 64 kg with its mass concentrated in the trunk, 0.19 m above the pelvis. The trunk's rotational inertia is about $2.2\,\mathrm{kg}\cdot\mathrm{m}^2$. Each leg of this bipedal robot is constructed from four lightweight carbon fiber segments. The proximal segments are driven in the sagittal plane by series elastic actuators (SEA) composed of a fiberglass leaf spring and a geared electric DC motor. The reflected inertia of these hip-anchored motors is about $3.75\,\mathrm{kg}\cdot\mathrm{m}^2$ after gearing. With a power supply stabilized by a 0.12 F electrolytic capacitor, these motors can draw peak currents of 165 A each, which translates into peak torques of about $600\,\mathrm{N}\cdot\mathrm{m}$ per actuator at the joint level. In addition, frontal plane abduction and adduction of each hip is provided by a third DC motor mounted on the trunk. Although ATRIAS is capable of untethered 3-D locomotion, this paper focuses on planar control theory of the SMM; hence, the trunk is attached to a boom but is free to pitch in the sagittal plane. The boom constrains the robot to move in a sphere and has negligible mass and inertia. The boom pivot point moves freely with the robot, and thus does not transmit any significant forces in the sagittal plane that could stabilize the trunk's pitch.

A. Implicit regulation of system energy

Two points complicate the transfer of control theories developed for the SMM onto legged robots such as ATRIAS. The first point is that the system energy is constant in the model but will change in a robot due to the desire to accelerate and brake as well as internal friction. One way of changing energy in the SMM is to introduce another control input, such as a variable leg stiffness during stance [16]. However, we adopt a different approach. We approximate the SMM dynamics (1) around the vertical pose $(x, z) = (0, z_0^*)$ with $z_0^* < l_0$ by

$$m\ddot{x} = k\left(z_0^* - z\right)\frac{x}{z}, \tag{3}$$

$$m\ddot{z} = k\left(z_0^* - z\right) - mg. \tag{4}$$

This approximate SMM is similar to the one used in [17]; it has decoupled vertical dynamics, which enables independent control of apex height and horizontal speed achieved during flight, implicitly regulating system energy with more natural gait variables. Specifically, we use (4) to prescribe a desired vertical motion $z^*(t)$ for ATRIAS with apex height z_a^* and landing and takeoff height z_0^* (Fig. 2). Given this reference, we compute the corresponding return map of the horizontal motion from (3). Thus, the updated deadbeat control law for leg placement in flight becomes

$$\alpha^*_{\mathrm{TD},i} = f^{-1}_{\mathrm{approx}}(\dot{x}_i, \dot{x}^*_a, z^*(t)), \tag{5}$$

which regulates running speed on ATRIAS.

Besides implicit regulation of system energy, the approximation of the SMM with (3) and (4) allows us to easily generalize this model from a point mass to a rigid body, which we address in the next section.

B. Explicit stabilization of trunk orientation

A second point complicating the transfer of SMM theories on to bipedal robots is that they require stabilization of trunk orientation, which is ignored in the SMM. This is a common problem in humanoid walking control based on the linear inverted pendulum model. It is often solved using a nonlinear quadratic program for a full order dynamics model of the

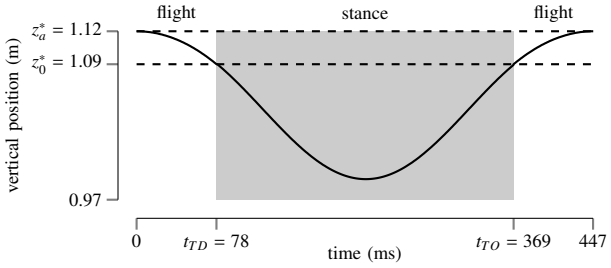

Fig. 2. Prescribed vertical motion $z^*(t)$ between two apexes. The motion is derived from (4) assuming $m = 64\,\mathrm{kg}$ and $k = 16\,\mathrm{kN \cdot m^{-1}}$ (details on the choice of k provided in Sec. IV-A). The motion is used by the ATRIAS controller as a target behavior and re-initiated in every flight phase.

robot [12]–[14]. This optimization balances different goals, such as the center of mass (CoM) behavior, trunk orientation, and other constraints on the robot motion. Due to computational costs, the optimization typically applies to only the current time step without taking advantage of future dynamics. In contrast to this approach, we introduce an intermediate model of reduced order (Fig. 3b) that allows us to consider the future dynamics of a floating rigid body with orientation θ, inertia I, and dynamics

$$\begin{aligned} m\ddot{x} &= F_x, \\ m\ddot{z} &= F_z - mg, \\ I\ddot{\theta} &= -zF_x + xF_z, \end{aligned} \tag{6}$$

using finite-horizon linear quadratic regulation (LQR), as detailed in section III-B. Here F_x and F_z are the ground reaction forces of the approximate SMM model modified by a stabilizing control for the trunk orientation (detailed in section III-B below, equation 9). We assume that the centralized inertia I on ATRIAS is constant, rather than configuration-dependent, because the robot's legs are light relative to its body.

C. Overview of control flow

Given the approximate spring mass model, the intermediate complexity model distributes translational and rotational motion. However, a third layer of model complexity is required to translate this centroidal motion into robot control. Overall this leads to a three layer control structure.

Figure 3 summarizes the flow of this control structure for the transfer of SMM control theory onto the ATRIAS biped. At the highest level, we define a spring mass gait based on desired speed and desired apex height. The corresponding approximate SMM provides the desired CoM trajectory in stance and the desired deadbeat angle in flight (Fig. 3a). In stance, the intermediate implementation level then generates GRFs that optimally trade off the desired CoM behavior against the desired trunk orientation (Fig. 3b). These GRFs are mapped in the next level by a dynamics model of the ATRIAS robot (detailed in [16]),

$$\boldsymbol{M}\ddot{\boldsymbol{q}} + \boldsymbol{h} = \boldsymbol{S}\,\boldsymbol{\tau} + \boldsymbol{J}^T\boldsymbol{F}, \tag{7}$$

to the required joint torques (Fig. 3c), which are finally converted into desired motor velocities for the torque control of ATRIAS's SEAs (Fig. 3d).

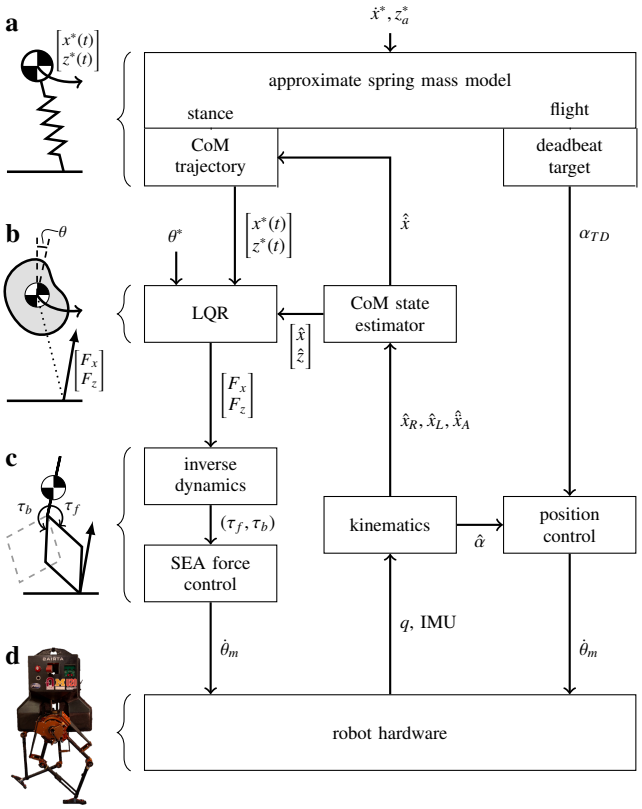

Fig. 3. Overview of implemented control. See section II-C for details.

In flight, the deadbeat angle from the approximate SMM is used to generate a foot point trajectory for the leg that achieves the target angle at a designated touchdown time (Fig. 2). This foot trajectory is converted into joint trajectories using a kinematics model of ATRIAS (Fig. 3c). The joints are then position-controlled by sending a velocity command to the robot SEAs (Fig. 3d).

III. IMPLEMENTATION

The control implementation on the ATRIAS biped requires more consideration. Besides detailing the individual layers of the control flow presented in the last section, this section explains how we address state estimation, external disturbances, and model inaccuracies. All described control is implemented onboard ATRIAS using MATLAB Simulink Realtime software with an update rate of 1 kHz.

A. Estimation of CoM and contact states

Tracking the CoM of ATRIAS and knowledge about its ground contact state are prerequisites for implementing the SMM control. For the first, we use two independent but identically structured Kalman filters estimating the horizontal and vertical CoM states. In both filters, the underlying model is a point mass m influenced by an applied force F. For instance,

the resulting discrete time process equation of the filter for the horizontal states is

$$\begin{bmatrix} x_{t+1} \\ \dot{x}_{t+1} \\ \ddot{x}_{t+1} \end{bmatrix} = \begin{bmatrix} 1 & \Delta t & 0 \\ 0 & 1 & \Delta t \\ 0 & 0 & 1 \end{bmatrix} \begin{bmatrix} x_t \\ \dot{x}_t \\ \ddot{x}_t \end{bmatrix} + \begin{bmatrix} 0 \\ 0 \\ \frac{1}{m} \end{bmatrix} (\hat{F}_t^x - \hat{F}_{t-1}^x) + \begin{bmatrix} 0 \\ 0 \\ \frac{1}{m} \end{bmatrix} w_t,$$

where $\Delta t = 1\,\text{ms}$ is the time step and w is Gaussian white process noise with covariance $Q = 25\,\text{N}^2$. The force $\hat{F}^x$ is estimated from the measured torques of the hip SEAs and the commanded torques of the lateral motors (ATRIAS has no torque sensing for its lateral motors). This is accomplished by solving for $\boldsymbol{F}$ in equation 7 with the constraint $\boldsymbol{J}\ddot{\boldsymbol{q}} = -\dot{\boldsymbol{J}}\dot{\boldsymbol{q}}$, which assumes a static point of contact, yielding the dynamics,

$$\hat{\boldsymbol{F}} = f_{\text{dyn}}(\hat{\boldsymbol{\tau}}, \boldsymbol{q}, \dot{\boldsymbol{q}}). \tag{8}$$

The measurement equation of the filter is

$$\begin{bmatrix} \hat{x}_t^R \\ \hat{x}_t^L \\ \hat{\ddot{x}}_t^A \end{bmatrix} = \begin{bmatrix} 1 & 0 & 0 \\ 1 & 0 & 0 \\ 0 & 0 & 1 \end{bmatrix} \begin{bmatrix} x_t \\ \dot{x}_t \\ \ddot{x}_t \end{bmatrix} + \mathbf{v_t},$$

where $\hat{x}^{L/R}$ are estimates of the horizontal distances from the left and right feet to the CoM, respectively, $\hat{\ddot{x}}^A$ is an estimate of the horizontal acceleration of the CoM, and $\mathbf{v}$ is measurement noise. The distances are computed from the kinematics model of ATRIAS using the robot's measured joint angles and trunk orientation. The acceleration is calculated using acceleration measurements from an IMU attached to ATRIAS's trunk. The horizontal filter is initialized using these measurements on every touchdown to account for a changing foot point. The vertical filter is only initialized once on the first touchdown. The covariance matrix

$$R_t = \frac{1}{\Delta t} \begin{bmatrix} R_{mx} - \mu_R(R_{mx} - R_{mn}) & 0 & 0 \\ 0 & R_{mx} - \mu_L(R_{mx} - R_{mn}) & 0 \\ 0 & 0 & R_A \end{bmatrix}$$

of the measurement noise is adaptive. Specifically, the covariance for the distance measurement noise is inversely proportional to the estimated load on each leg in units of body weight, $\mu_{R/L} = 10\,\hat{F}^z_{R/L}/(mg)$ ($\mu_{R/L}$ clamped to $[0, 1]$, $R_{mn} = 5 \times 10^{-5}\,\text{m}^2$, $R_{mx} = 1\,\text{m}^2$, and $R_A = 4\,\text{m}^2/\text{s}^4$).

The contact state of each leg is determined from the estimated vertical GRF, $\hat{F}_z$. ATRIAS has no explicit contact or force sensing at its feet; instead, the force estimate (8) is used to determine if a leg is in stance. An $\hat{F}_z$ exceeding 50% of body weight triggers the touchdown event and causes the control to enter the stance phase. Conversely, once the vertical CoM velocity $\hat{\dot{z}}$ crosses from negative to positive values, indicating rebound, a drop in $\hat{F}_z$ below the 50% threshold triggers take off and the exit from stance control. This threshold level creates a small delay of approximately 15 ms (about 5% of stance duration) in contact detection.

B. Stance control

Upon transition of ATRIAS into the stance phase, the approximate SMM layer of the control (Fig. 3a) generates a desired CoM trajectory $[x^*(t),\, z^*(t)]$ based on the previous takeoff velocity $\hat{\dot{x}}_i$, the next desired takeoff velocity $\dot{x}^*_{i+1}$, the prescribed vertical motion $z^*(t)$, and equation (3) (Sec. II-A). Note, although $x^*(t)$ describes the horizontal motion in stance, it is chosen along with the foot placement based on the system state at the previous takeoff. The layer also generates a corresponding force input $\mathbf{u}^*(t) = [F_x^*(t),\, F_z^*(t)]$ from the GRFs of the approximate SMM with $F_z^*(t) = k(z_0^* - z^*(t))$ and $F_x^*(t) = F_z^*(t)\, x^*(t)/z^*(t)$.

In the second control layer (Fig. 3b), the force input is modified to account for trunk stabilization. The desired CoM trajectory is combined with a desired trunk orientation $\theta^*(t) = 0$ into a reference motion $\boldsymbol{\xi}^*(t) = [x^*(t),\, \dot{x}^*(t),\, \theta^*(t),\, \dot{\theta}^*(t),\, z^*(t),\, \dot{z}^*(t)]$ for a floating rigid body (Sec. II-B). We convert the floating rigid body dynamics (equation 6) to state space form and linearize the error dynamics around this reference trajectory, which yields,

$$\Delta\dot{\boldsymbol{\xi}} = \begin{bmatrix} 0 & 1 & 0 & 0 & 0 & 0 \\ 0 & 0 & 0 & 0 & 0 & 0 \\ 0 & 0 & 0 & 1 & 0 & 0 \\ \frac{F_z^*(t)}{I} & 0 & 0 & 0 & -\frac{F_x^*(t)}{I} & 0 \\ 0 & 0 & 0 & 0 & 0 & 1 \\ 0 & 0 & 0 & 0 & 0 & 0 \end{bmatrix} \Delta\boldsymbol{\xi} + \begin{bmatrix} 0 & 0 \\ 1/m & 0 \\ 0 & 0 \\ \frac{-z^*(t)}{I} & \frac{x^*(t)}{I} \\ 0 & 0 \\ 0 & 1/m \end{bmatrix} \Delta\boldsymbol{u},$$

where $\Delta\boldsymbol{\xi} = \boldsymbol{\xi} - \boldsymbol{\xi^*}$ and $\Delta\boldsymbol{u} = \boldsymbol{u} - \boldsymbol{u^*}$. We approximate $F_x^*(t) = 0$ and $x^*(t) = 0$, which decouples the vertical state error dynamics. As this approximate model is linear, finite horizon LQR yields the optimal force control input $\mathbf{u}(t) = \mathbf{u}^*(t) - \mathbf{K}(t)(\boldsymbol{\xi}(t) - \boldsymbol{\xi}^*(t))$ for trading off tracking the SMM behavior against balancing the trunk, with the feedback gain $\mathbf{K}(t) = [\mathbf{K}_x(t), \mathbf{K}_z]$. Thus, the second control layer generates the modified desired GRF $\mathbf{u}(t) = [F_x(t), F_z(t)]$ with components

$$F_x = F_x^* - \mathbf{K}_x \begin{bmatrix} x - x^* \\ \dot{x} - \dot{x}^* \\ \theta - \theta^* \\ \dot{\theta} - \dot{\theta}^* \end{bmatrix}, \quad F_z = F_z^* - \mathbf{K}_z \begin{bmatrix} z - z^* \\ \dot{z} - \dot{z}^* \end{bmatrix}. \tag{9}$$

The third control layer (Fig. 3c) converts the desired GRFs (9) into motor commands of the robot's SEAs in three steps. First, the forces are passed through a safety check to ensure that the foot does not slip on the ground. This requires the vertical force to remain positive, $F_z \geq 0$, and the horizontal force F_x to be inside a friction cone with stiction coefficient of 0.5. It is important to note that these two constraints are almost never active on ATRIAS because stance begins when F_z exceeds 50% of body weight (Sec. III-A) and the stance leg is typically near the vertical. Second, the control compensates for the vertical constraint forces caused by the boom (Fig. 1), $F_z^\dagger = F_z\hat{F}_z/(m\hat{\ddot{z}})$, where $\hat{\ddot{z}}$ is provided by the CoM state estimator (Sec. III-A). Third, the modified desired forces, $F_x^\dagger$ and $F_z^\dagger$, are then mapped based on the dynamics model of ATRIAS (7) into joint torques using

$$\boldsymbol{\zeta} = \begin{bmatrix} \mathbf{M}_{5\times5} & -\mathbf{S}_{5\times2} \\ \mathbf{J}_{2\times5} & \mathbf{0}_{2\times2} \end{bmatrix}^{-1} \left(\begin{bmatrix} \mathbf{h}_{5\times1} \\ -(\dot{\mathbf{J}}\dot{\mathbf{q}})_{2\times1} \end{bmatrix} + \begin{bmatrix} \mathbf{J}^T_{5\times2} \\ \mathbf{0}_{2\times2} \end{bmatrix} \begin{bmatrix} F_x^\dagger \\ F_z^\dagger \end{bmatrix} \right)$$

with $\boldsymbol{\zeta} = [\ddot{x}\ \ddot{z}\ \ddot{\theta}\ \ddot{l}\ \ddot{\gamma}_l\ \tau_f\ \tau_b]^T$ specifying accelerations as well as joint torques, and $\ddot{l}$ and $\ddot{\gamma}_l$ being the leg length and angle accelerations, respectively (detailed in [16]). Although the solution vector $\boldsymbol{\zeta}$ contains both accelerations and torques, the accelerations are not used by the controller. Furthermore, because the swing leg is light, we do not account for its

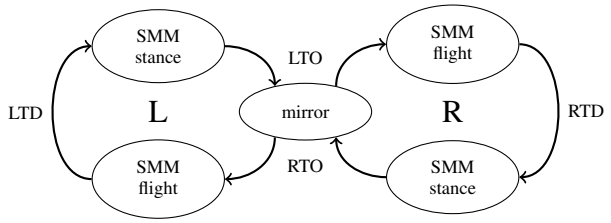

Fig. 4. State-machine of ATRIAS biped control. While the left (L) or right (R) leg cycles through an SMM flight and stance phase, the other leg remains in the transitory mirror phase. Both legs switch roles when take off occurs. TD/TO: touchdown/takeoff.

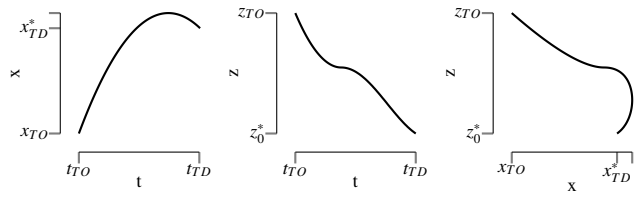

Fig. 5. Desired foot point trajectory in the flight control phase. The horizontal trajectory is a quadratic function. The vertical trajectory is composed of a quadratic function, which increases z_{flight} to encourage leg retraction, and a cosine function to approach the landing condition.

accelerations and control it independently as described in the next section. Finally, the resulting joint torques, τ_f and τ_b, are tracked on ATRIAS using the velocity-based SEA controller described in [18].

C. Flight control

Once ATRIAS transitions out of stance, the SMM prescribes only a desired landing angle $\alpha^*_{\text{TD},i}$ (5). The model does not specify which of the robot's two legs is to land or how it shall reach the target. We solve the first problem by introducing a transitory control phase and the second by defining a kinematic trajectory for the foot point.

Figure 4 summarizes the state machine of the ATRIAS controller. While one leg follows the SMM stance and flight behaviors, the other leg remains in a mirror control phase. For instance, when the right leg takes off (RTO), it enters this mirror phase and the left leg simultaneously transitions from it into the flight control phase. The right leg remains in the mirror phase while the left leg cycles through an entire step until it takes off (LTO), at which point both legs switch roles.

When a leg is in the mirror control phase, its motion reflects that of the other leg. Raibert [5] introduced this concept of symmetric leg motion, which reduces trunk pitching and prepares the leg for landing. Specifically on ATRIAS, we reflect the foot-to-CoM reference $[x^*(t), z^*(t)]$ from the simplified model (Sec. III-B) across the line $x = 0$. We then negate this reflection to transform it into a CoM-to-foot trajectory,

$$\boldsymbol{r}_{\text{mirror}}(t) = \left[\, x^*(t)\,,\, -\left(z^*(t) \,-\, \rho\right) \right],$$

where $\rho = 0.2\,\text{m}$ ensures leg retraction for ground clearance.

When a leg switches into the flight control phase at takeoff time t_{TO}, a new CoM-to-foot trajectory is engaged,

$$\boldsymbol{r}_{\text{flight}}(t) = \left[x_{\text{flight}}(t)\,,\, z_{\text{flight}}(t)\right],$$

where $x_{\text{flight}}(t)$ and $z_{\text{flight}}(t)$ are analytic functions that guide the foot to the desired landing condition at a predicted touchdown time $\hat{t}_{\text{TD}}$ (Fig. 5). These functions begin at the takeoff mirror position, $\boldsymbol{r}_{\text{mirror}}(t_{\text{TO}})$, and end at the desired deadbeat landing position, $\boldsymbol{r}_{\text{flight}}(\hat{t}_{\text{TD}}) = -[z^*_0/\tan(\alpha^*_{\text{TD},i}), z^*_0]$. The velocity at the expected touchdown time is chosen to match the ground speed, $\dot{\boldsymbol{r}}_{\text{flight}}(\hat{t}_{\text{TD}}) = [-\dot{\hat{x}}_{\text{TO}}, 0]$, based on the estimated horizontal velocity at takeoff. The predicted touchdown time

$$\hat{t}_{\text{TD}} = \frac{\dot{\hat{z}}_{\text{TO}}}{g} + \frac{1}{g}\sqrt{\dot{\hat{z}}^2_{\text{TO}} - 2g(z^*_0 - \hat{z}_{\text{TO}})}$$

is calculated from the expected touchdown state (Sec. II-A) and from the estimated (Sec. III-A) vertical CoM position $\hat{z}_{\text{TO}}$ and velocity $\dot{\hat{z}}_{\text{TO}}$ at takeoff.

Both the mirror and flight foot trajectories are mapped through the kinematics model of ATRIAS into leg joint trajectories $\mathbf{q}(t)$ that are tracked with position control (Fig. 3c). Here the compliance of the SEAs is ignored by assuming the motor output shafts are rigidly connected to the joints.

D. Online adaptation of return map

The final piece of control implementation is the online adaptation of the deadbeat control (5) derived from the approximate SMM. To counter small systematic modeling errors and imperfect torque tracking of ATRIAS, the observed error in the return map behavior of ATRIAS is approximated by a linear model

$$\dot{\hat{x}}_{i+1} - \dot{x}^*_a = \epsilon_1 \dot{x}^*_a + \epsilon_0, \tag{10}$$

where $\dot{\hat{x}}_{i+1}$ is the observed speed in the flight phase $i+1$ and ϵ_0 and ϵ_1 are obtained online through linear regression,

$$\begin{bmatrix}\epsilon_1 \\ \epsilon_0\end{bmatrix} = (X^T X)^{-1} X^T Y,$$

with $X_i = [\dot{x}^*_a\ 1]$ and $Y_i = \dot{\hat{x}}_{i+1} - \dot{x}^*_a$. This error is compensated for by adapting the landing angle. For small deviations, the return map of the approximate SMM generates an error

$$\dot{x}_{i+1} - \dot{x}^*_a = \partial_{\dot{x}} f^* \left(\dot{x}_i - \dot{x}^*_a\right) + \partial_\alpha f^* \left(\alpha_{TD,i} - \alpha^*_{TD,i}\right)$$

with the partial derivatives pre-computed from the SMM return map. Hence, the observed error (10) is compensated for by the adapted landing angle,

$$\alpha^\dagger_{TD,i} = \alpha^*_{TD,i} - \left(\epsilon_1 \dot{x}^*_a + \epsilon_0 + \partial_{\dot{x}} f^* \left(\dot{x}_i - \dot{x}^*_a\right)\right) / \partial_\alpha f^*.$$

IV. HARDWARE EXPERIMENTS

To evaluate the planar running control developed in sections II and III, we perform several experiments on undisturbed and disturbed locomotion using the ATRIAS biped attached to the boom (Fig. 1 and supplementary video). In this setup, power is supplied to the robot externally; however, all sensing and computation is performed on-board. Each experiment starts with ATRIAS standing still in a reference pose on one leg. A human operator then holds the boom to stabilize the robot while it follows a reference chirp signal for its CoM height. When takeoff occurs, the actual controller engages and the operator releases the boom. Besides the constant apex height

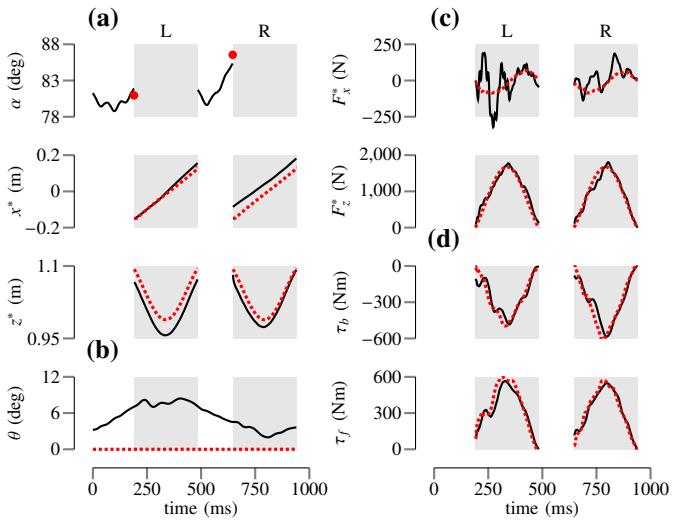

Fig. 6. Tracking performance of implemented controller for ATRIAS running at $1\,\mathrm{m}\cdot\mathrm{s}^{-1}$ over flat ground without gait disturbances. Shown are the desired (red dashed) and observed trajectories (black solid) of key control variables (Fig. 3) for two consecutive steps. The asymmetry between the left (L) and right leg (R) occurs due to the boom constraint.

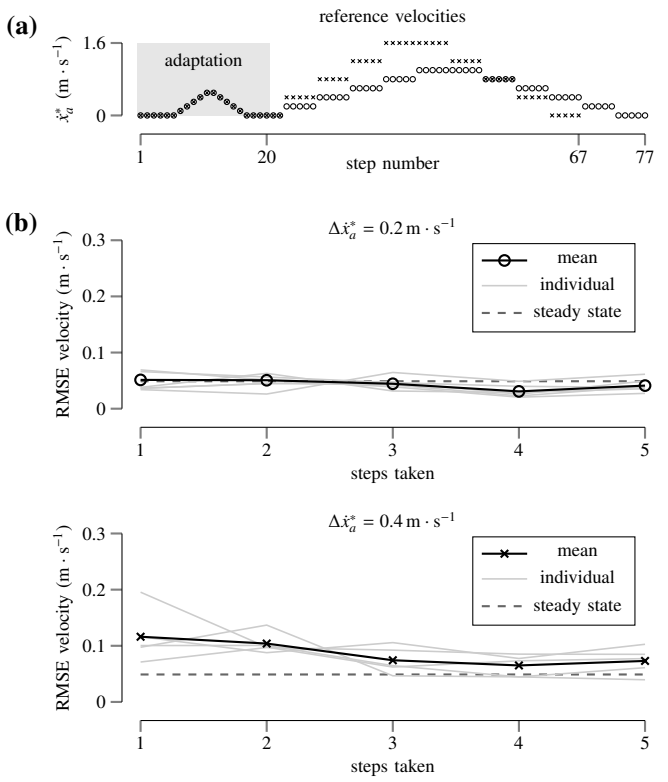

Fig. 7. Tracking of SMM deadbeat velocity targets. (a) Profile of desired apex velocities $\dot{x}_a^*$ for changes of $0.2\,\mathrm{m}\cdot\mathrm{s}^{-1}$ (circles) and $0.4\,\mathrm{m}\cdot\mathrm{s}^{-1}$ (crosses). The first 20 steps are used in each trial for the online adaptation of the return map (Sec. III-D) and do not count toward the experiments. (b) Root-mean-square error between the target velocity and the robot's velocity in flight over the number of consecutive steps taken after a change in the velocity target. Averages over all five trials are shown for the entire experiment (black) and separated out based on the different trials (gray). The dashed line indicates the average tracking error in undisturbed locomotion at $1\,\mathrm{m}\cdot\mathrm{s}^{-1}$ (Sec. IV-A).

target z_a^* (Fig. 2), the input provided in each trial by the operator to the ATRIAS controller is a profile of apex velocity targets $\dot{x}_a^*$ indexed by step number. The first and last velocity targets are always zero, and each experiment ends once the robot reaches the last step.

A. Undisturbed running

First, we evaluate the performance of the proposed controller in undisturbed running over level ground at a speed of $1\,\mathrm{m}\cdot\mathrm{s}^{-1}$. In this gait, about 80% of the available torque of ATRIAS's SEAs is consumed for generating the desired spring mass rebound behavior (eqs. 3 and 4) with a stiffness $k = 16\,\mathrm{kN}\cdot\mathrm{m}^{-1}$. This stiffness optimally trades off longer stance phases (larger vertical impulses) against the reduced mechanical advantage of ATRIAS's legs with increasing compression [19]. As a result, it enables the largest hopping heights of about 3 cm with appreciable flight times of about 150 ms (Fig. 2). The remaining 20% of torque capacity is available for error compensation. ATRIAS utilizes a large amount of torque to achieve this gait due to the low mechanical advantage in its legs. Other similarly sized robots with different geometries would require different torques, but the ground reaction forces for this spring mass behavior would remain the same.

The tracking performance of the controller is summarized in figure 6. At the SMM level, the controller tracks the desired CoM trajectory $[x^*(t), z^*(t)]$ in stance with an error (mean and standard deviation) of 4.5 ± 4.7 cm in x and 2.6 ± 2.0 cm in z, and tracks the target leg angle at touchdown with an error of 0.99 ± 0.80 ° (Fig. 6a). The model deviations originate from two primary sources. The first source is the GRF tracking error due to ground impacts, delayed contact detection, and limited actuator bandwidth. These force errors are reflected in the tracking of the desired SEA torques (53 ± 68 N · m error, Fig. 6d), which is limited by a 20 Hz closed-loop bandwidth of ATRIAS's SEAs. The second source is the stance feedback control, which creates deviations from the simplified model in order to stabilize the trunk orientation (error of 7.6 ± 6.2 °, Fig. 6b) as shown by the deviation in the GRF from the reference GRF of the SMM (error 110 ± 130 N, Fig. 6c).

B. Tracking SMM deadbeat velocity targets

In a second series of experiments we quantify how closely the implemented controller can realize the deadbeat behavior of the theoretical SMM model when the desired velocity $\dot{x}_a^*$ changes. We perform two sets of five repeated trials, in which ATRIAS runs over flat ground with desired apex velocities that change every five steps (Fig. 7a). In the first set, the change is $0.2\,\mathrm{m}\cdot\mathrm{s}^{-1}$ with a maximum base velocity of $1.0\,\mathrm{m}\cdot\mathrm{s}^{-1}$. In the second set, the change and maximum base velocity are $0.4\,\mathrm{m}\cdot\mathrm{s}^{-1}$ and $1.6\,\mathrm{m}\cdot\mathrm{s}^{-1}$, respectively. Larger step sizes require deadbeat foot targets beyond the mechanical limits of ATRIAS at high velocities. These limits impose a maximum possible velocity of $2.6\,\mathrm{m}\cdot\mathrm{s}^{-1}$ for the chosen spring mass gait.

The observed velocity tracking performance is summarized in figure 7b. ATRIAS tracks desired velocity changes of $0.2\,\mathrm{m}\cdot\mathrm{s}^{-1}$ (circles) with the average error observed in undisturbed running ($0.05\,\mathrm{m}\cdot\mathrm{s}^{-1}$, dashed line; compare Sec. IV-A) after one step, indicating spring-mass-like deadbeat behavior

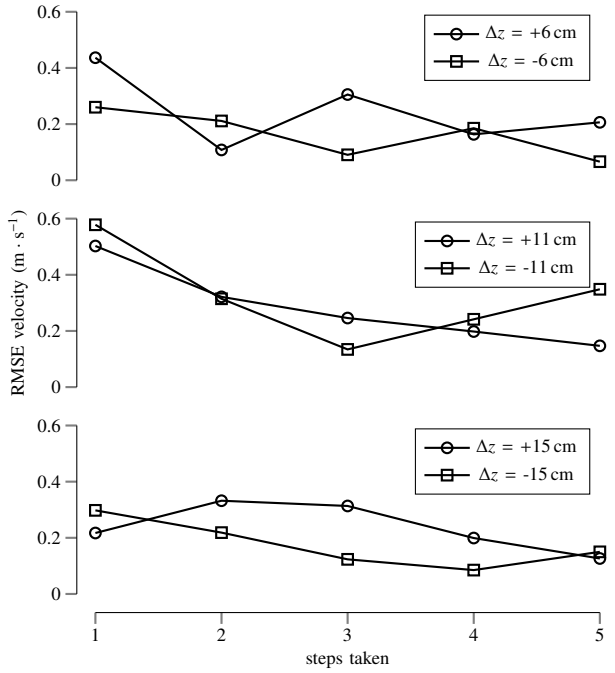

Fig. 8. Ground disturbance rejection. Shown are the averages over three trials for the root-mean-square error between the desired velocity $x_d^* = 1.0\,\mathrm{m \cdot s^{-1}}$ and the velocity achieved by the robot during flight over the number of consecutive steps taken after experiencing an unexpected ground height change Δz.

within the performance bounds of undisturbed gait. However, the robot requires more steps for tracking $0.4\,\mathrm{m \cdot s^{-1}}$ changes (crosses), caused mainly by increased ground impacts at the higher horizontal velocities. We measure a peak horizontal impact force of approximately 200 N when running at $1.0\,\mathrm{m \cdot s^{-1}}$. This impact force increases to nearly 300 N when running at $1.6\,\mathrm{m \cdot s^{-1}}$.

As described in section IV-A, the deviations from the simplified model are due to force tracking errors and trunk stabilization. For comparison to the hardware results, we quantify these two sources of deviation in simulation. When the simplified model is simulated with the same force errors measured on hardware, we observe similar velocity tracking errors of up to $0.15\,\mathrm{m \cdot s^{-1}}$ at $1.6\,\mathrm{m \cdot s^{-1}}$. When the intermediate complexity model (Fig. 3b) is simulated with an initial orientation error of 10°, we observe a velocity error of $0.05\,\mathrm{m \cdot s^{-1}}$ after one step. The system completely recovers after three steps. Thus, errors in force tracking and trunk orientation lead to a substantial performance deterioration compared to the SMM deadbeat control theory. This suggests that performance could be improved by extending the simplified model to account for ground impacts and rotational dynamics of the center body in legged locomotion.

C. Rejecting unexpected ground changes

With the third series of experiments, we explore how closely the implemented controller follows the deadbeat behavior of the SMM when the robot encounters unexpected changes in ground height. We perform experiments for six different ground height changes of ±6 cm, ±11 cm and ±15 cm, each repeated for three trials. In all trials, ATRIAS encounters the ground disturbance while running at $1.0\,\mathrm{m \cdot s^{-1}}$ with its reference gait. (Sec. IV-A).

Figure 8 shows the velocity tracking performance of ATRIAS after encountering a ground height change measured as the error in velocity over the steps taken. Deadbeat behavior would result in an error no larger than the average error of $0.05\,\mathrm{m \cdot s^{-1}}$ observed in undisturbed running at $1.0\,\mathrm{m \cdot s^{-1}}$ from the first step on. However, each of the ground height changes results in a substantial velocity error in the first step of about the same size ($0.2\,\mathrm{m \cdot s^{-1}}$ to $0.4\,\mathrm{m \cdot s^{-1}}$), which only gradually diminishes in the next steps.

The velocity error and its gradual decay are largely independent of the direction and size of the ground height change, which seems counterintuitive. For instance, a height drop of 15 cm results in an increase in speed to $2\,\mathrm{m \cdot s^{-1}}$ if maintaining the same total system energy. Similarly, a height increase of the same amount cannot be achieved without increasing system energy, even with zero speed. Comparing the two cases, it seems they should lead to very different behaviors, and thus velocity errors, after the disturbance.

The reason why the errors behave similarly is because they are due to the increased ground impacts and trunk orientation errors that are common to all of the height changes. The sudden ground height changes are implemented as sheer jumps in the floor surface using concrete blocks (Fig. 1). This leads to increased impact forces of nearly 500 N and swing foot impacts with the side of the elevated ground. Thus, most of the observed performance degradation compared to the SMM deadbeat control theory is again due to the increased ground impacts and required trunk stabilization. The detrimental effect of swing leg impacts suggests that hardware implementations should focus on more compliant swing leg motions than stiff kinematic control provides.

V. CONCLUSION

We investigated if the SMM leg placement theory can be transferred to running robots beyond the simplified one-legged test platforms used in previous studies. Specifically, we have evaluated the utility of spring mass theory on a robot of human scale and weight with an actively controlled trunk, articulated legs, and without external sensing. To this end, we focused on the ATRIAS biped platform and implemented on it a controller that transfers the SMM behavior through model-based force control in stance and kinematic control of foot placement in flight. We found that the proposed controller achieves on ATRIAS SMM-like deadbeat performance for velocity changes up to $\pm 0.2\,\mathrm{m \cdot s^{-1}}$. For larger velocity changes and for ground height changes ranging from ±6 cm to ±15 cm, the controller performance degraded, albeit without compromising gait robustness. The degradation was in large part due to ground impacts and the incessant need to stabilize the robot's trunk, neither of which are considered in the SMM theory. The results highlight the limited utility of this theory for the control of more complex running machines; on the other hand, they also point to the potential of such an SMM-based control for generating robust and versatile behavior in running robots.

The achieved performance mirrors the performance observed for the implementation of SMM-based deadbeat control strategies on the much simpler robot platforms. The velocity tracking error of 5% on ATRIAS during undisturbed running is in line with the results obtained by Zeglin, who demonstrated deadbeat hopping with a mean velocity error of approximately 15% between steps [9]. The ability of the proposed controller to tolerate unobserved rough terrain of at least 17% of the nominal leg length (0.9 m) is similar to the performance described by Shemer and Degani [10], who demonstrated deadbeat hopping over terrain height changes of about 15% of leg length. In contrast to the previous results, however, the demonstration of these capabilities on ATRIAS with similar performance shows that they generalize to more complex and human-like bipedal robots.

One key advantage of the model-based control framework [12]–[14] also pursued in this work is that it is easier to generalize behavior beyond scripted motions. For example, the MABEL robot is capable of planar running using a control framework based on hybrid zero dynamics. However, as the robot encounters perturbations, its controller must adapt speed to maintain stability leading to "considerable variation" in forward velocity [6]. Similarly, Hubicki and colleagues [8] discovered that ATRIAS is capable of 3-D running (although with very short flight phases of about 30 ms) when a heuristic controller designed for walking was commanded higher desired velocities. In contrast, our proposed controller can (within the bounds provided by the torque capacity of the actuators) freely choose the speed at which it runs from step to step, whether on flat ground or after a disturbance, by taking advantage of the underlying gait model and its deadbeat foot placement strategies.

Several research directions will help to further the model-based control framework for running robots. First, the SMM theory remains to be evaluated on robots running in 3-D environments. Second, performance degradation due to force errors and trunk stabilization suggests that the utility of the SMM theory could be increased by extending it to account for ground impacts and the rotational dynamics of a trunk. These force errors could also be mitigated by designing a more compliant swing leg control. Third, the mechanical limits of real robots prevent reaching certain target states in a single step. Robustness could potentially be improved in this case by considering these actuation limits [20], [21]. Finally, the transfer of SMM-based control to walking robots could substantially enlarge the range of robust behaviors that can be addressed. It is our goal to pursue these research directions in order to demonstrate highly robust 3-D running and walking on ATRIAS over uncertain terrain.

References

[1] U. Saranli, W. J. Schwind, and D. E. Koditschek, "Toward the control of a multi-jointed, monoped runner," in *Robotics and Automation, 1998. Proceedings. 1998 IEEE International Conference on*, vol. 3. IEEE, 1998, pp. 2676–2682.

[2] A. Seyfarth, H. Geyer, and H. Herr, "Swing-leg retraction: a simple control model for stable running," *Journal of Experimental Biology*, vol. 206, no. 15, pp. 2547–2555, 2003.

[3] S. G. Carver, N. J. Cowan, and J. M. Guckenheimer, "Lateral stability of the spring-mass hopper suggests a two-step control strategy for running," *Chaos: An Interdisciplinary Journal of Nonlinear Science*, vol. 19, no. 2, p. 026106, 2009.

[4] A. Wu and H. Geyer, "The 3-d spring–mass model reveals a time-based deadbeat control for highly robust running and steering in uncertain environments," *IEEE Transactions on Robotics*, vol. 29, no. 5, pp. 1114–1124, 2013.

[5] M. H. Raibert, *Legged robots that balance*. MIT press, 1986.

[6] K. Sreenath, H.-W. Park, I. Poulakakis, and J. Grizzle, "Embedding active force control within the compliant hybrid zero dynamics to achieve stable, fast running on mabel," *The International Journal of Robotics Research*, vol. 32, no. 3, pp. 324–345, 2013.

[7] D. J. Hyun, S. Seok, J. Lee, and S. Kim, "High speed trot-running: Implementation of a hierarchical controller using proprioceptive impedance control on the mit cheetah," *The International Journal of Robotics Research*, vol. 33, no. 11, pp. 1417–1445, 2014.

[8] C. Hubicki, A. Abate, P. Clary, S. Rezazadeh, M. Jones, A. Peekema, J. Van Why, R. Domres, A. Wu, W. Martin, H. Geyer, and J. Hurst, "Walking and running with passive compliance: Lessons from engineering a live demonstration of the atrias biped," *IEEE Robotics and Automation Magazine*, 2016.

[9] G. Zeglin, "The bow leg hopping robot," Ph.D. dissertation, Carnegie Mellon University, 1999.

[10] N. Shemer and A. Degani, "Analytical control parameters of the swing leg retraction method using an instantaneous slip model," in *2014 IEEE/RSJ International Conference on Intelligent Robots and Systems*. IEEE, 2014, pp. 4065–4070.

[11] İ. Uyanık, Ö. Morgül, and U. Saranli, "Experimental validation of a feedforward predictor for the spring-loaded inverted pendulum template," *IEEE Transactions on Robotics*, vol. 31, no. 1, pp. 208–216, 2015.

[12] S. Feng, E. Whitman, X. Xinjilefu, and C. G. Atkeson, "Optimization-based full body control for the darpa robotics challenge," *Journal of Field Robotics*, vol. 32, no. 2, pp. 293–312, 2015.

[13] T. Koolen, S. Bertrand, G. Thomas, T. De Boer, T. Wu, J. Smith, J. Englsberger, and J. Pratt, "Design of a momentum-based control framework and application to the humanoid robot atlas," *International Journal of Humanoid Robotics*, vol. 13, no. 01, p. 1650007, 2016.

[14] S. Kuindersma, R. Deits, M. Fallon, A. Valenzuela, H. Dai, F. Permenter, T. Koolen, P. Marion, and R. Tedrake, "Optimization-based locomotion planning, estimation, and control design for the atlas humanoid robot," *Autonomous Robots*, vol. 40, no. 3, pp. 429–455, 2016.

[15] C. Hubicki, J. Grimes, M. Jones, D. Renjewski, A. Spröwitz, A. Abate, and J. Hurst, "Atrias: Design and validation of a tether-free 3d-capable spring-mass bipedal robot," *The International Journal of Robotics Research*, p. 0278364916648388, 2016.

[16] A. Wu and H. Geyer, "Highly robust running of articulated bipeds in unobserved terrain," in *2014 IEEE/RSJ International Conference on Intelligent Robots and Systems*. IEEE, 2014, pp. 2558–2565.

[17] I. Mordatch, M. De Lasa, and A. Hertzmann, "Robust physics-based locomotion using low-dimensional planning," in *ACM Transactions on Graphics (TOG)*, vol. 29, no. 4. ACM, 2010, p. 71.

[18] A. Schepelmann, M. D. Taylor, and H. Geyer, "Development of a testbed for robotic neuromuscular controllers," *Robotics: Science and Systems VIII*, 2012.

[19] W. C. Martin, A. Wu, and H. Geyer, "Robust spring mass model running for a physical bipedal robot," in *2015 IEEE International Conference on Robotics and Automation (ICRA)*. IEEE, 2015, pp. 6307–6312.

[20] M. Ernst, H. Geyer, and R. Blickhan, "Extension and customization of self-stability control in compliant legged systems," *Bioinspiration & biomimetics*, vol. 7, no. 4, 2012.

[21] T. Cnops, Z. Gan, and C. D. Remy, "The basin of attraction for running robots: Fractals, multistep trajectories, and the choice of control," in *Intelligent Robots and Systems (IROS), 2015 IEEE/RSJ International Conference on*. IEEE, 2015, pp. 1586–1591.